X-ray Structure of Ornithine Decarboxylase from *Trypanosoma brucei*: The Native Structure and the Structure in Complex with α-Difluoromethylornithine[†,‡]

Nick V. Grishin,[§,||] Andrei L. Osterman,[§,⊥] Harold B. Brooks,[§,#] Margaret A. Phillips,*[,§] and Elizabeth J. Goldsmith*[,▽]

Departments of Pharmacology and Biochemistry, The University of Texas Southwestern Medical Center at Dallas, 5323 Harry Hines Boulevard, Dallas, Texas 75235

Received June 30, 1999; Revised Manuscript Received August 23, 1999

ABSTRACT: Ornithine decarboxylase (ODC) is a pyridoxal 5′-phosphate (PLP) dependent homodimeric enzyme. It is a recognized drug target against African sleeping sickness, caused by *Trypanosoma brucei*. One of the currently used drugs, α-difluoromethylornithine (DFMO), is a suicide inhibitor of ODC. The structure of the *T. brucei* ODC (TbODC) mutant K69A bound to DFMO has been determined by X-ray crystallography to 2.0 Å resolution. The protein crystallizes in the space group $P2_1$ (a = 66.8 Å, b = 154.5 Å, c = 77.1 Å, β = 90.58°), with two dimers per asymmetric unit. The initial phasing was done by molecular replacement with the mouse ODC structure. The structure of wild-type uncomplexed TbODC was also determined to 2.9 Å resolution by molecular replacement using the TbODC DFMO-bound structure as the search model. The N-terminal domain of ODC is a β/α-barrel, and the C-terminal domain of ODC is a modified Greek key β-barrel. In comparison to structurally related alanine racemase, the two domains are rotated 27° relative to each other. In addition, two of the β-strands in the C-terminal domain have exchanged positions in order to maintain the location of essential active site residues in the context of the domain rotation. In ODC, the contacts in the dimer interface are formed primarily by the C-terminal domains, which interact through six aromatic rings that form stacking interactions across the domain boundary. The PLP binding site is formed by the C-termini of β-strands and loops in the β/α-barrel. In the native structure Lys69 forms a Schiff base with PLP. In both structures, the phosphate of PLP is bound between the seventh and eighth strands forming interactions with Arg277 and a Gly loop (residues 235−237). The pyridine nitrogen of PLP interacts with Glu274. DFMO forms a Schiff base with PLP and is covalently attached to Cys360. It is bound at the dimer interface and the δ-carbon amino group of DFMO is positioned between Asp361 of one subunit and Asp332 of the other. In comparison to the wild-type uncomplexed structure, Cys-360 has rotated 145° toward the active site in the DFMO-bound structure. No domain, subunit rotations, or other significant structural changes are observed upon ligand binding. The structure offers insight into the enzyme mechanism by providing details of the enzyme/inhibitor binding site and allows for a detailed comparison between the enzymes from the host and parasite which will aid in selective inhibitor design.

Ornithine decarboxylase (ODC)[1] catalyzes the first committed step in the biosynthesis of the polyamines (*1*). The polyamines are ubiquitous to all cells and are required for cell growth and differentiation. Inhibitors of polyamine biosynthesis arrest cell growth and have been used clinically for the treatment of *Trypanosoma brucei*, the causative agent of African sleeping sickness, *Pneumocystis* pneumonia in AIDS patients, and cancer (*2*−*4*). ODC was identified as a drug target against *T. brucei* by the discovery that the ODC inhibitor, α-difluoromethylornithine (DFMO), cures *T. brucei* infection in mice (*5*) and man (*6*). The growth requirement of *T. brucei* for ODC has been demonstrated by study of an ODC knockout cell line that is unable to grow in the absence of putrescine (*7*).

Currently, 50 million people are at risk from infection by *T. brucei*, yet the available antitrypanosomal drugs are limited in effectiveness (*6*). Despite the success of DFMO against *T. brucei gambiense*, the pharmacokinetics of DFMO are

[†] This work was supported by grants (to M.A.P.) from the National Institutes of Health (R01 AI34432), the Welch Foundation (I-1257), and the Burroughs Wellcome Fund, (to H.B.B.) from the National Institutes of Health (F32 AI09495), and (to E.J.G.) from the Welch Foundation (I-1128).

[‡] Coordinates for the structures of *T. brucei* K69A ODC bound to DFMO and of native ODC have been deposited in the Protein Data Bank with the PDB ID codes 2tod and 1QU4.

* To whom correspondence should be addressed. Tel: M.A.P., (214) 648-3637; E.J.G., (214) 648-5009. Fax: M.A.P., (214) 648-9961; E.J.G., (214) 648-8954. E-mail: M.A.P., philli01@utsw.swmed.edu; E.J.G., betsy@howie.swmed.edu.

[§] Department of Pharmacology.

[||] Present address: National Center for Biotechnology Information, NIH, Bethesda, MD 20894.

[⊥] Present address: Integrated Genomics Inc., 2201 W. Campbell Park Drive, Chicago, IL 60612.

[#] Present address: Ely Lilly Co., Lilly Corporate Center, Indianapolis, IN 46285.

[▽] Department of Biochemistry.

[1] Abbreviations: ODC, ornithine decarboxylase; TbODC, *Trypanosoma brucei* ornithine decarboxylase; AR, alanine racemase; PLP, pyridoxal 5′-phosphate; DFMO, α-difluoromethylornithine; RMSD, root-mean-square deviation.

10.1021/bi9915115 CCC: $18.00
Published on Web 10/30/1999

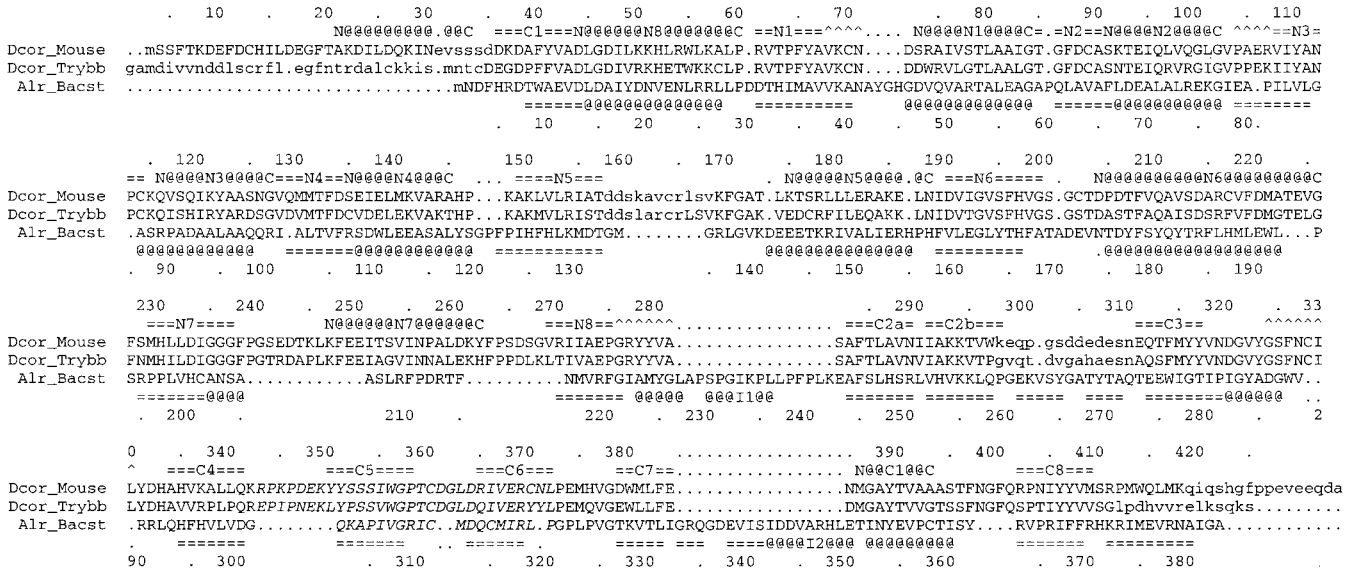

FIGURE 1: Structure-based sequence alignment of *T. brucei* ODC (Dcor_Trybb), mouse ODC (Dcor_Mouse), and AR from *B. stearothermophilus* (Alr_Bacst). Dots in the sequences represent gaps in the alignment. Residues not present in the coordinate files are in lower case letters. Sequence numbers and secondary structural elements are shown for TbODC (above the alignment) and AR (below the alignment): @, α-helical residue; =, *β*-strand residue [with number of secondary structural elements (N for N-terminal domain, C for C-terminal domain) shown in the middle]; ∧, 3_{10}-helix. α-Helices are flanked by N-cap (N) and C-cap (C). Letters in italic correspond to the region of the hairpin flip.

relatively poor, and clinical isolates of the more virulent *T. brucei rhodesiense* are naturally resistant to DFMO. Thus, there is a need to develop novel ODC inhibitors that can overcome these shortcomings. A structure-based approach for designing novel inhibitors of protein function has been used to generate clinically useful drugs against a number of human diseases (*8*−*10*). However, application of this method requires a detailed knowledge of the target protein's structure and function.

ODC is a pyridoxal 5′phosphate (PLP) dependent enzyme. Eukaryotic ODC is a distant structural homologue of alanine racemase (AR), which requires the same cofactor, and it is not related to the bacterial ODCs [Figure 1 (*11*)]. We previously predicted that the N-terminal domain of both ODC and AR would have a *β*/α-barrel structure (*11*). This finding was first confirmed by solution of the X-ray structure of AR (*12*) and recently by the solution of the X-ray structure of the native mouse ODC (*13*). This structure additionally reveals that the C-terminal domain of ODC folds into a *β*-barrel with topology slightly different from that observed in AR. In this paper we describe the 2.0 Å structure of the K69A mutant of *T. brucei* ODC bound to the irreversible inhibitor DFMO. The structure was solved by molecular replacement using the mouse ODC coordinates (*13*). In addition, the structure of the wild-type uncomplexed *T. brucei* enzyme was solved to 2.9 Å by molecular replacement from the DFMO-bound *T. brucei* ODC structure.

EXPERIMENTAL PROCEDURES

Protein Expression and Purification. ODC was expressed as an N-terminal 6xHis-tag fusion protein including the TEV-protease cleavage site from a T7 promoter in *Escherichia coli* BL21(DE3) cells as described (*14*). Protein was purified by Ni^{2+}-NTA−agarose followed by Superdex 200 gel-filtration column chromatography. The 6xHis-tag was removed by treatment with TEV-protease immobilized on glutathione−agarose to produce ODC with a native N-terminus as described (*15*). Tag-minus ODC was recovered in the flow-through of the Ni^{2+}-NTA−agarose column and applied to a Superdex 200 gel-filtration column. The protein eluted from this last step was homogeneous by SDS−PAGE and was concentrated to 20−25 mg/mL for crystallization experiments.

Crystallization. Crystallization conditions were identified in Hampton crystallization screens [Riverside, CA (*16*)]. The uncomplexed ODC was crystallized as described previously (*15*). The DFMO-complexed ODC crystals were prepared as follows: ODC (20 mg/mL ODC in 10 mM HEPES−NaOH, pH 7.2, 50 mM NaCl, 0.5 mM EDTA, 0.015% Brij35, 10 mM DTT) was preincubated with DFMO (0.02 M) for 10 min at room temperature before crystallization. The crystals were obtained at 16 °C by vapor diffusion, mixing equal volumes of DFMO-inactivated ODC and well solution [16% PEG 3350, 0.2 M Na(CH_3COO), 100 mM HEPES, pH 7.5]. This procedure resulted in mostly twinned and stacked crystals, which were used for microseeding into the solution of the above content. Plate-shaped single crystals grew close to the surface of the drop within a few days.

Data Collection and Processing. Diffraction data were collected at 90 K on FUJI image plates at beam line A1 at the Cornell High Energy Synchrotron Source (CHESS) (DFMO complex) and at the X12C beam line with MAR detector at the Brookhaven Synchrotron source (uncomplexed ODC). Data were processed and scaled using DENZO and SCALEPACK (*17*). A summary of the data processing statistics is given in Table 1.

Structure Determination and Refinement. Initial phases for the DFMO-complexed structure were calculated from a molecular replacement solution [program AMoRe (*18*)] obtained using mouse ODC (coordinates were provided by Dr. Marvin Hackert) as the search model. Mouse ODC shares 61% sequence identity with *T. brucei* and gave a 13.9 σ peak for each monomer in the rotation function and a 7.1 σ peak for the first monomer in the translation function. The rotation

Table 1: Data Collection, Processing, and Refinement Statistics for *T. brucei* ODC Structure Determination

	K69A−DFMO complex	native
(a) data collection and processing		
data source	beam line A1 at CHESS	beam line X12C at Brookhaven
wavelength (Å)	0.908	0.91
temperature (K)	90	90
resolution (Å)	40.0−2.0	20.0−2.9
total reflections	339850	120960
unique reflections	103282	36421
completeness (%) (last shell $I > \sigma$)	97.6 (61.7)	98.6 (75.3)
multiplicity	3.3	3.3
intensities I/σ (last shell)	13.9 (1.9)	14.3 (5.0)
R_{merge}	0.09	0.08
(b) refinement		
no. of reflections ($F > 1\sigma$)	101011 (8.0−2.0 Å)	34588 (8.0−2.9 Å)
no. of non-H protein atoms	10142	10130
no. of water molecules	869	0
$R_{crystal}$ (%)/R_{free} (%) ($F > 2\sigma$)	21.2/27.0 (8.0−2.0 Å)	23.0/27.6 (8.0−2.9 Å)
$R_{crystal}$ (%)/R_{free} (%) ($F > 2\sigma$)	20.5/26.6 (8.0−2.1 Å)	22.8/26.8 (8.0−3.0 Å)
$R_{crystal}$ (%)/R_{free} (%) ($F > 2\sigma$)	30.8/34.7 (2.09−2.0 Å)	24.7/34.8 (3.0−2.9 Å)
RMSD bond lengths (Å)	0.016	0.013
RMSD bond angle distances (Å)	0.041	0.039
average *B*-values (Å^2)	35.7	30.4

solution was particularly strong, because crystal packing resulted in transitional symmetry between the two dimers in the asymmetric unit, as revealed from the self-Patterson function. Rigid body refinement yielded an *R*-factor of 41% and a correlation coefficient of 62% for resolution between 10 and 3 Å. The resulting map, calculated using SIGMAA weights with REFMAC in CCP4 (*19*) revealed interpretable electron density. The model was built in O (*20*). The structure was refined in REFMAC (*21*) using maximum likelihood refinement, X-PLOR (*22*), and later CNS (*23*−*25*) using molecular dynamics and energy minimization on data between 8.0 and 2.0 Å. Once R_{free} was below 35%, individual *B*-factors were refined. A bulk solvent correction allowed the inclusion of data between 20 and 2.0 Å. The tight noncrystallographic symmetry constraints were kept (except for the region 200−207) until the last round of refinement. The peptide torsion angles for 1067 out of 1206 well-defined non-glycine residues fall within the most favored regions of the Ramachandran plot, as defined in the program PROCHECK (*26*). There are no residues in disallowed regions. The structure of the uncomplexed wild-type TbODC was solved by molecular replacement from the DFMO-complexed TbODC structure using the same methods. Rigid body refinement yielded an *R*-factor of 34.5% (10−3.0 Å). The model was edited in O (*20*) and refined with REFMAC (*21*) under strict NCS constraints on data between 20.0 and 2.9 Å. No water molecules were added.

RESULTS

Crystallization, Data Collection, and Structure Determination. Crystallization of TbODC was attempted for both native and mutant TbODC, with and without bound inhibitors, with the goal of optimizing the diffraction limit. Crystals of native TbODC were obtained in space group $P2_1$ (a = 66.3 Å, b = 151.8 Å, c = 83.7 Å, β = 101.2°) as described [diffraction limit 2.9 Å resolution (*15*)]. However, better quality crystals were obtained for the K69A mutant of TbODC in complex with DFMO (diffraction limit 2.0 Å resolution). DFMO is a suicide inhibitor of ODC [K_I = 160 mM, k_{inact} = 0.6 s^{-1} (*27*)]. The mechanism by which DFMO inactivates ODC has been studied by peptide mapping; 80% of the DFMO was found covalently bound to Cys360 and 20% was bound through Lys69 (*28*). The TbODC K69A mutant was used for crystallization to avoid heterogeneity of labeling with DFMO. The K69A mutant has a k_{cat} for L-Orn that is 10^4-fold lower than that for the wild-type enzyme, while K_m remains unchanged (*29*). The rate of the decarboxylation step has been reduced to a similar extent as the overall k_{cat} by this mutation; thus inactivation of K69A ODC by DFMO most likely occurs at a significantly reduced rate compared to wild-type ODC. However, given the incubation time of the crystallization experiment, complete labeling of the mutant enzyme is readily achieved. As was observed for the uncomplexed wild-type enzyme, DFMO-bound K69A TbODC crystallized in space group $P2_1$ (a = 66.8 Å, b = 154.5 Å, c = 77.1 Å, β = 90.58°), with two TbODC homodimers occupying the asymmetric unit and 32% solvent.

The structure of K69A TbODC bound to DFMO was solved by molecular replacement, using the structure of mouse ODC (*13*) as the search model. The final model comprises 1424 residues of four noncrystallographic symmetry-related TbODC protein chains, 4 PLP, 4 DFMO, and 869 water molecules. The R-factor is 21.1% (R_{free} = 27.0%) (Table 1) for 8.0−2.0 Å resolution ($F > 2\sigma$) data, with the model constrained to preserve noncrystallographic symmetry, with the exception of amino acids 200−207. The release of the noncrystallographic symmetry constraints aided in model building of residues 200−207. This loop participates in crystal contacts and exhibits two conformations. The 2.0 Å electron density map for TbODC, near the active site region, is shown in Figure 2. Although the electron density map for most of the residues is unambiguous, 70 residues could not be interpreted. These regions include the N-terminus (residues 1−35), the C-terminus (residues 412−425), and two loops (residues 158−165 and 298−310). Most of these regions were not observed in the final model of the mouse ODC structure either. The density for the region from residues 342−348, which forms a long loop, was poor but interpretable with *B*-factors above 70 Å^2.

The structure of native TbODC was solved by molecular replacement using the refined DFMO-bound K69A TbODC

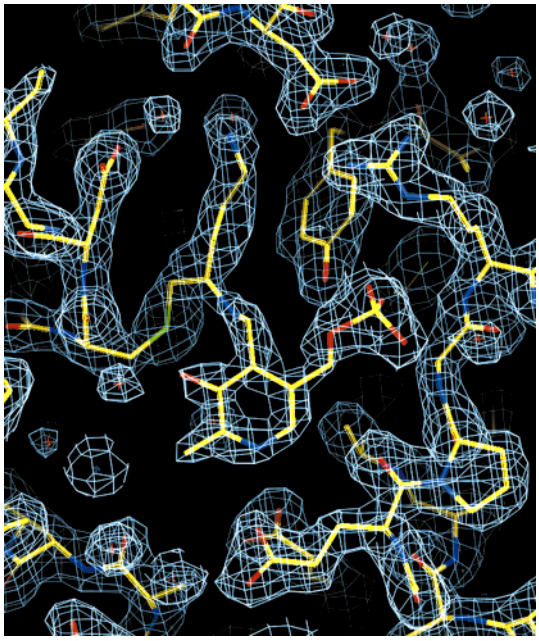

FIGURE 2: Electron density map of the TbODC active site region. The σ_a-weighted $2F_o - F_c$ electron density map of the active site region is contoured at 1.1σ.

structure. The *R*-factor is 23.0% (R_{free} = 27.6%) (Table 1) for 8.0−2.9 Å resolution ($F > 2\sigma$) data with the model constrained to preserve noncrystallographic symmetry. No water molecules were added.

General Structure Description. The TbODC monomer is composed of two domains, an N-terminal β/α-barrel and a C-terminal modified Greek key β-sheet domain (Figure 3a). The four TbODC monomers in the asymmetric unit form two 2-fold symmetric dimers. The dimer is an elliptical disk with dimensions 90 Å × 70 Å × 40 Å, and the two active sites are on the same face of the disk (Figure 4). Unlike classical β/α-barrels, the N-terminal domain of TbODC begins with an α-helix and ends with a β-strand (Figure 1). The barrel is elliptical with an axial ratio of 1.5. The longest axis segregates strands N2−N5 from strand N1 and N6−N8. Helices N1−N4 of the TbODC barrel are shorter (three turns) than helices N5−N8 (four to six turns). The pseudo-8-fold rotation axes of the two β/α-barrels are at an angle of 60° with the 2-fold axis of a dimer and nearly occupy the same plane. The C-terminal domain (residues 35−42 and 285−410) β-barrel is six-stranded and possesses a single cross-over connection. Strands C3 and C5 are parallel, and there is no hydrogen bonding between strands C4 and C6, opening the barrel. The β-barrel in ODC contains several insertions: two long loops (residues 297−312 and 341−349), a 3_{10} helix (residues 323−331), a partially distorted α-helix (residues 387−394), and two additional strands, C1 and C8. Strands C1 and C8 are parallel to each other and extend the antiparallel sheet formed by strands C2a, C4, and C7.

The uncomplexed TbODC structure is highly similar to the DFMO-bound TbODC structure, even in the crystal packing. Comparison of dimer to dimer and monomer to monomer yields an RMSD of 0.5 and 0.45 Å between 716 and 358 C_α atoms, respectively.

Subunit Interface. The subunit interface is formed by interactions between the C-terminal domains of opposite subunits (Figure 5a) and by interactions of the C-terminal domain of one monomer with the N-terminal domain of the other (Figure 5b). In total 2775 Å^2 are buried in the interface. The most prominent feature in the contact between C-terminal domains is a row of aromatic rings (aromatic amino acid zipper) that passes through the 2-fold axis (Figure 5a). The rings of PheA397, TyrA323, and PheB331 are involved in a stacking interaction. At the 2-fold axis, Tyr331 from one subunit is oriented with the ring perpendicular to the Tyr331 ring from the other subunit. The distal aromatic residues of the zipper contact DFMO in the two active sites. On the opposite face of the dimer a segment of residues in an extended conformation (392−397) forms an antiparallel interaction. However, these segments make only two β-sheet hydrogen bonds. The interaction between the C-terminal domain of one monomer with the N-terminal domain of the other monomer houses the active site (Figure 5b). The subunit interactions in this section of the subunit interface are partially hydrophilic and include salt bridges between LysA169 and AspB364 and between AspA134 and LysB294.

PLP Binding Site. Residues from three domains, both domains of one monomer and the β-barrel domain of the other, participate in each active site. PLP is bound inside the N-terminal β/α-barrel domain close to strands N6−N8 (residue numbers 197−200, 233−237, and 274−277; Figure 3a). The phosphate binding site is formed by the N-terminus of a short helix after strand N8, with Arg277 involved in a charge interaction (Figure 6). In addition, Gly237 N, Ser200 O_γ and Tyr389 O_η hydrogen bond to the phosphate oxygens. Only Tyr389 comes from the C-terminal domain. The other phosphate binding residues are supplied by the β/α-barrel. The aromatic ring of the PLP interacts with the side chain of His197, with the plane of the ring at a 30° angle with the PLP ring system. The N_1 atom of PLP forms a hydrogen bond with one of the side chain oxygens of Glu274. The O_3 atom of PLP interacts with Arg154 through a well-ordered water molecule, W3. In the uncomplexed TbODC structure, the N_Z of Lys69 forms a Schiff base with PLP, and the conformation of the Lys69 side chain is similar to that observed in mouse ODC (*13*).

Substrate Binding Site. Within a single active site, DFMO bridges between the two subunits forming a Schiff base with the PLP on one monomer and a covalent bond to Cys360 (atom S_γ) of the other monomer (Figure 6). The side chain of DFMO is in the extended conformation. The N_ϵ of DFMO forms a hydrogen bond to AspA332 $O_{\delta1}$ (2.9 Å) and water-mediated hydrogen bonds to AspB361 $O_{\delta1}$ (through W1) and TyrB323 O_η (through W2). The aliphatic portion of DFMO is cradled by the aromatic rings of PheB397 and TyrA389. Thus the side chain is bound at the dimer interface with residues from both subunits contributing to enzyme−inhibitor interactions. The only significant difference between the DFMO-bound and uncomplexed TbODC active sites involves a 145° rotation of Cys360 toward the active site upon binding DFMO (Figure 7).

DISCUSSION

Comparison of the DFMO-Bound T. brucei ODC Structure with the Uncomplexed Structure. The DFMO-bound and uncomplexed TbODC structures are very similar, not only in the packing of molecules in the unit cell but also in the

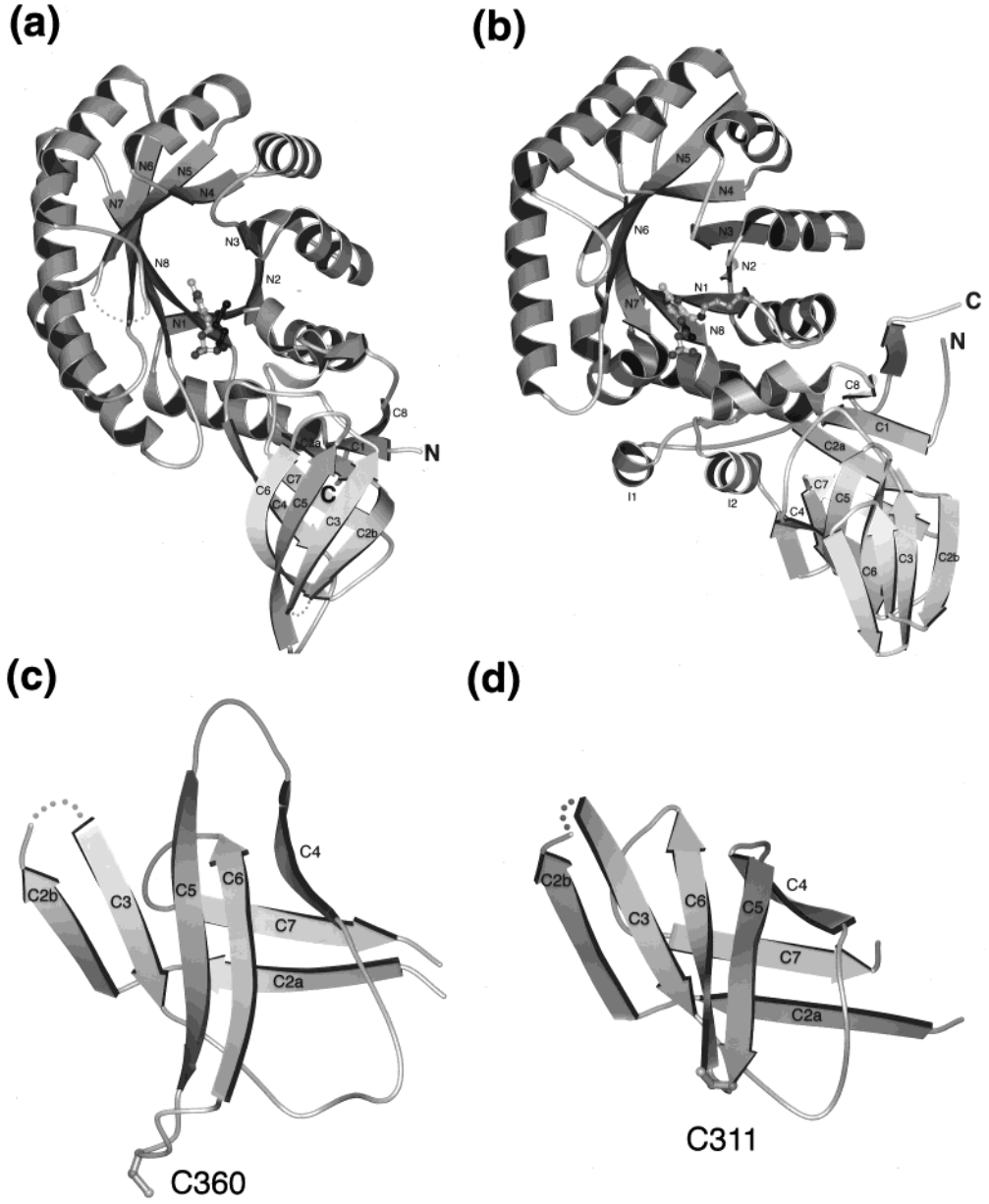

FIGURE 3: (a) Ribbon diagram of the TbODC monomer. (b) Ribbon diagram of the AR monomer (1sft; ref *12*). Strands are numbered according to their position in the sequence (Figure 1). PLP, DFMO in TbODC, and acetate in AR are displayed as ball-and-stick models. The core regions of the TbODC (c) and AR (d) β-barrel domains are shown. The conserved Cys residue is displayed in ball-and-stick representation. The pictures are drawn by Bobscript and rendered by PovRay (*55, 56*).

details of the structures (Figure 7). There are no differences in crystal packing in the contact-forming regions, no local conformational changes in loop regions, and no global domain movements. Indeed, the domain orientation and the monomer arrangement within the dimer are the same. This implies the absence of monomer movement in ODC, upon substrate binding, in contrast to other PLP-dependent enzymes [e.g., aspartate aminotransferase (*30*)]. The side chain position of Lys69 can only be determined from the native TbODC structure because it is mutated to Ala in the DFMO-complexed structure. The only significant difference between the two structures is in the side chain orientation of Cys360 (Figure 7). Cys360 is rotated away from the active site in the uncomplexed structure and toward the active site in the DFMO-bound structure, forming a covalent bond with DFMO. This Cys360 side chain rotation is likely to be of functional importance, since rotation places the SH group within 4 Å of the Schiff base nitrogen. In the DFMO-bound structure, Cys360 is in position to act as a general acid to protonate the C_α carbon after decarboxylation or to influence the orientation of the L-Orn carboxylate (Figure 6). In support of the latter, mutation of Cys to Ala decreases k_{cat} by 50-fold and ^{13}C isotope studies suggest that the mutation has decreased the rate of the decarboxylation step (*31*).

ODC from T. brucei and Mouse: More Similarities than Differences. Mouse and *T. brucei* ODC share 61% sequence identity (*32*), and the structures can be superimposed with an RMSD of 0.8 Å over 350 C_α atoms (Figure 8). This level of structural similarity is typical for what has been observed for proteins with closely related sequences (*33*−*35*). The active site region is highly conserved, and the variable residues are largely confined to the surface (Figure 4b). Furthermore, there are no subunit or domain movements between the mouse and the two *T. brucei* ODC structures.

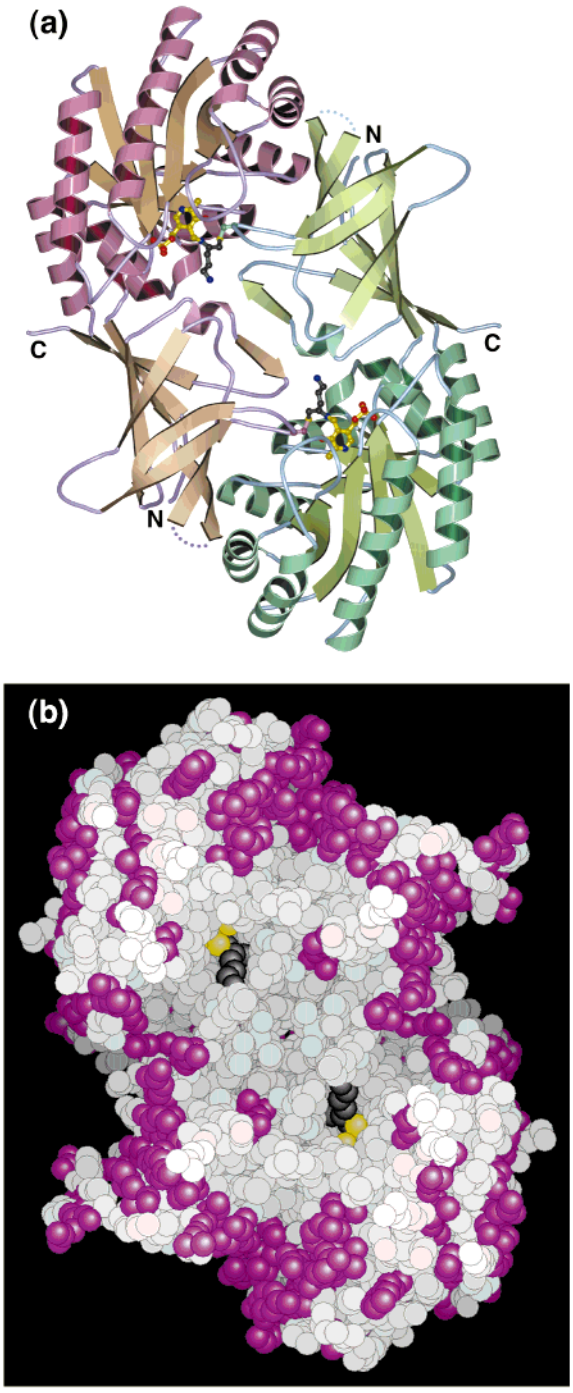

FIGURE 4: (a) Ribbon diagram of the TbODC dimer drawn by Bobscript and rendered by PovRay (*55*, *56*). Monomers are shown in pink and green. The N- and C_α-termini are labeled. PLP and DFMO are shown in ball-and-stick representation. The C_α atoms of PLP are in yellow, and the C_α atoms of DFMO are in black. (b) Space-filling model of the TbODC dimer drawn by GRASP (*57*). Residues that are invariant between mouse and TbODC are displayed in white, residues that are not conserved between the two structures are in purple, PLP is displayed in yellow, and DFMO is displayed in black.

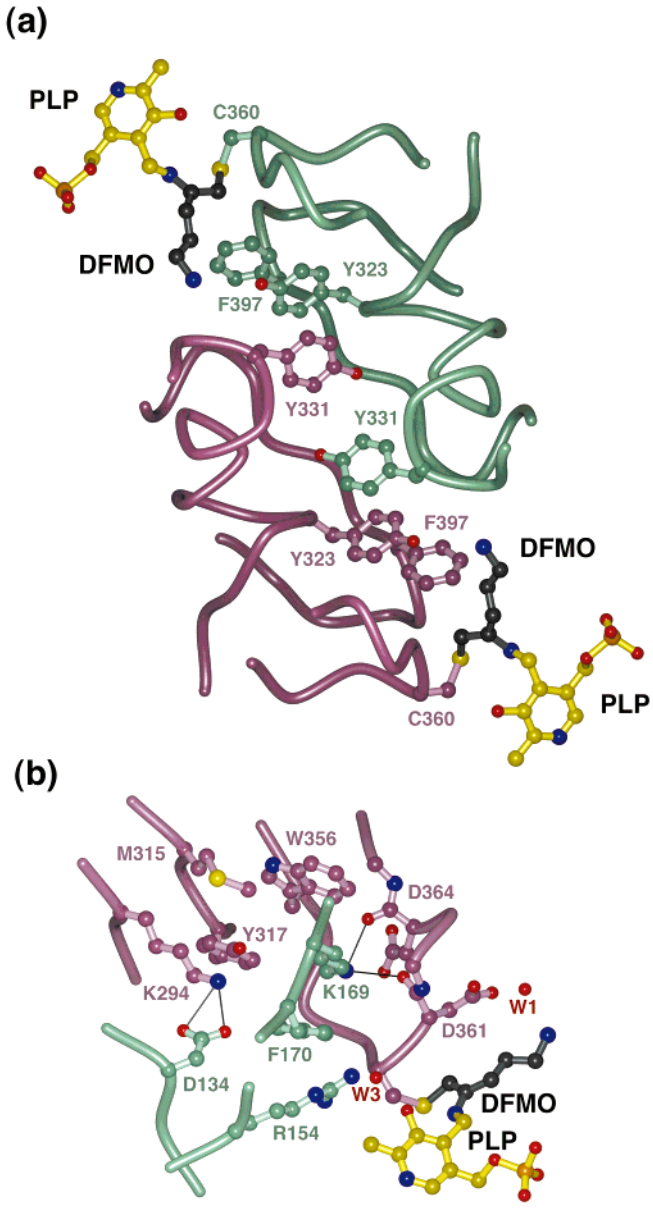

FIGURE 5: Dimer interface of TbODC. (a) Interface between the two C-terminal domains. (b) Interface between the C-terminal domain of one subunit and the N-terminal domain of the other. PLP and DFMO are shown in ball-and-stick representation. Monomers are colored pink and green.

The largest main chain differences map to the three regions that form lattice contacts (residues 199−206, 242−246, and 265−268). In addition, few differences in side chain conformations are found in the active site structure. The position of Cys360 is identical between the two uncomplexed structures (mouse and TbODC). A small difference is observed in the His197 ring, which is positioned at a 30° angle to the PLP ring for TbODC, while in the mouse ODC structure the His197 ring is almost parallel to the PLP ring.

ODC and AR: Distant Homologues. TbODC and AR from *Bacillus stearothermophilus* share 17% sequence identity based on a structure-derived sequence alignment (Figure 1). Both consist of two domains: a β/α-barrel and a β-barrel (Figure 3a,b). The β/α-barrels in TbODC and AR superimpose with an RMSD of 3.0 Å; the C-terminal domains superimpose with an RMSD of 3.5 Å (residues in superpositions are indicated in Roman upper case letters on Figure 1). When the β/α-barrels are optimally superimposed, the C-terminal domains in ODC and AR are related by a 27° rotation.

The C-terminal β-barrel domains of ODC and AR are similar but not identical in topology (Figure 3c,d). The AR β-barrel is a typical Greek key (*36*), similar to the N-terminal domain of α and β subunits of F1 ATP synthase (*37*). ODC differs from AR in placement of strands C5 and C6. Strands

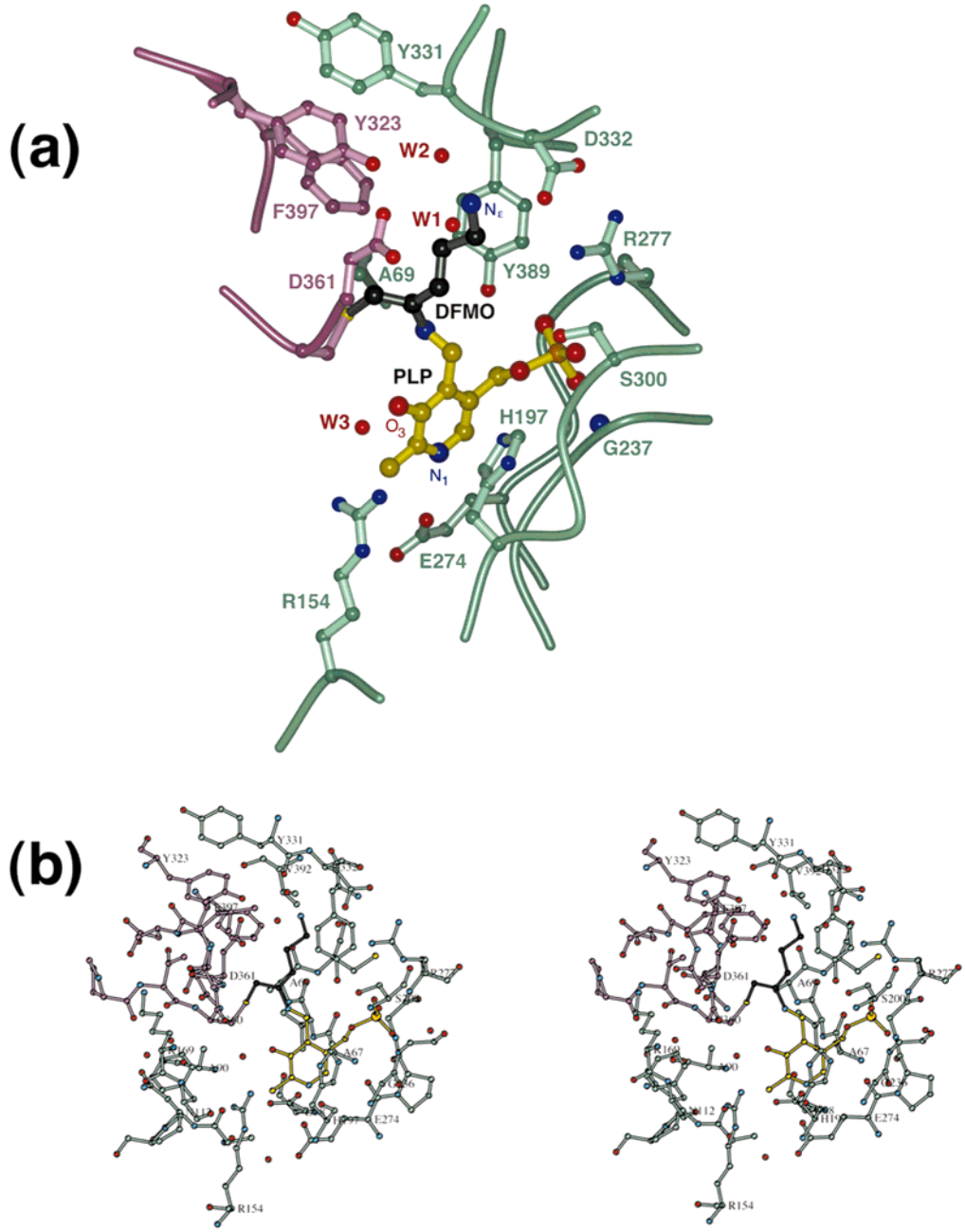

FIGURE 6: Active site of K69A TbODC in complex with DFMO. (a) Selected residues in the active site region. Residues from different subunits are colored pink and green. The C_α atoms of PLP are in yellow, the C_α atoms of DFMO are in black, nitrogen atoms are in blue, and oxygen atoms are in red. (b) Stereoview of the active site. All residues within 10 Å from the Schiff base nitrogen are shown.

C3 and C5 form parallel H-bonding in ODC, while there is no H-bonding between strands C4 and C6, the minimum distance between the strands being 6 Å. In AR, strand C3 interacts with strand C6 in an antiparallel fashion. Antiparallel hydrogen bonding exists between strands C4 and C5 as well. The 180° rotation of the hairpin formed by residues 350−373 in ODC places strand C6 within hydrogen-bonding distance to strand C3, thereby restoring the AR topology. Thus, ODC and AR apparently represent an example of homologous proteins with structures of different topology. Though rare, a hairpin flip has also been observed as a difference between the structures of the homologous proteins triabin and lipocalin (*38, 39*).

Despite the topological difference, regions involved in the hairpin flip show stronger sequence similarity than the remainder of the C-terminal domain (Figure 1). The functionally important Cys360 residue in ODC (Cys311 in AR) is found at the tip of the hairpin and occupies a similar position relative to other active site residues in the β/α-barrel domain of the two enzymes. This is accomplished by a β-barrel domain rotation between ODC and AR. Indeed, optimal superposition of the β/α-barrels results in a superposition of the C5 strands, with the conserved Cys following these strands (Figure 3c,d) and with the rest of the second domain structure about 27° away. The hairpin flip allows the positioning of strand C5, in relation to the first domain, to be preserved. The positioning of the second domain may be due to lack of helices I1 and I2 in ODC.

Correlation of Biochemical Data with the Structure: the PLP Binding Site. Site-directed mutagenesis, kinetic studies,

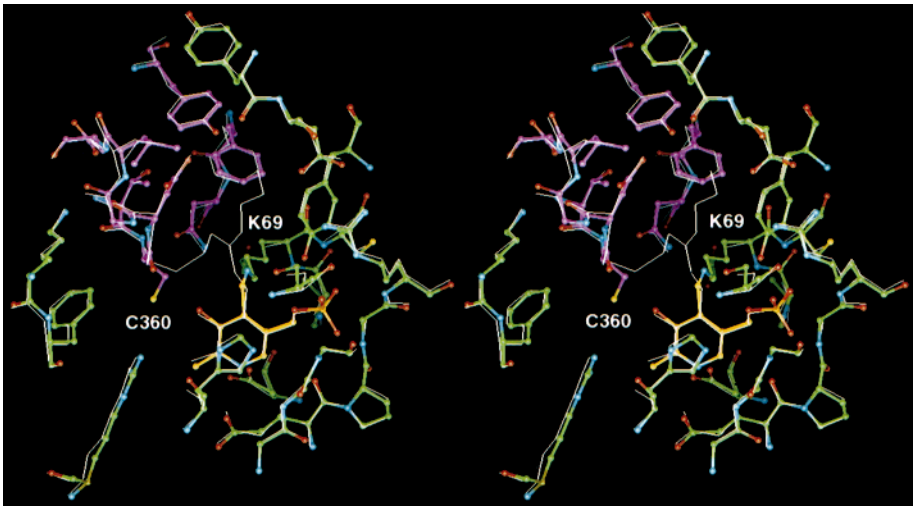

FIGURE 7: Stereoview of the superposition of TbODC K69A bound to DFMO (thin white line) and uncomplexed TbODC (ball and stick), where the C_α of one monomer is in green and the other is in pink. PLP is in yellow. Positions with significant difference are labeled.

FIGURE 8: Stereoview of the superposition of TbODC K69A DFMO (thicker lines) and mouse ODC (thinner lines) monomers. Numbers, corresponding to TbODC, are shown to the right of the C_α atoms. Side chains of His197, Ser200, and Cys360 are shown in both structures. The picture was generated by Bobscript (*55, 56*).

and computer modeling provided significant information about the catalytic mechanism of ODC prior to the X-ray structure solution. We previously proposed a model of the PLP binding site of ODC on the basis of the structure of FMN binding barrels (*11*). The X-ray structure of TbODC demonstrates that the positions of the main PLP binding residues (Lys69, Arg154, His197, Gly235−Gly237, Glu274, and Arg277) were predicted correctly in the model.

Lys69 forms a Schiff base with PLP in the uncomplexed TbODC (Figure 7) and mouse ODC (*13*) structures. This residue has been shown to be essential for multiple steps in the catalytic cycle; the rates of the Schiff formation, decarboxylation, and product release steps are all decreased 10^3-10^4-fold by mutation of this residue (*29, 31*). Comparison of the DFMO-bound TbODC K69A structure with the uncomplexed TbODC structure demonstrates that no structural changes in nearby residues or in the domain or subunit structure have occurred as a result of this mutation (Figure 7).

The X-ray structure demonstrates that Glu274 forms a hydrogen bond to the N_1 of PLP, confirming its role in stabilizing a charge at this position. Mutation of Glu274 to Ala decreases k_{cat} by 50-fold; however, activity of the E274A ODC mutant is restored if *N*-methylpyridoxal 5′-phosphate, which fixes the positive charge on N_1, is substituted as the cofactor. These data suggested that the role of Glu274 is to increase the electron-withdrawing properties of the ring by enhancing the basicity of the pyridine nitrogen (*40*). This function is similar to that observed for other PLP-dependent enzymes that have an acidic residue interacting with the pyridine nitrogen of PLP [e.g., aspartate aminotransferase (*30, 41*)].

The phosphate binding site is formed by Arg277 and by the Gly-rich loop (235−237). Mutation of Arg277 to Ala decreased the PLP binding affinity for ODC by >20-fold and altered the ^{31}P NMR spectrum arising from ODC-bound PLP (*42*). Thus, the interaction between Arg277 and the 5′-phosphate of PLP, observed in the X-ray structure, is

important for the energetics of PLP binding. The X-ray structure also shows that Tyr389 forms a hydrogen bond with the PLP phosphate and that Arg277 is also involved in substrate binding as a second-shell residue. A salt bridge is formed between Arg277 and Asp332 (2.9 Å), the residue that forms a hydrogen bond with N_ϵ of DFMO (Figure 6).

The functions of other conserved PLP binding site residues are less well understood. In TbODC, His197 is positioned against PLP (30° between rings); a His residue occupies this position in most PLP-dependent enzymes. His197 plays an essential catalytic role in ODC, as mutation of this residue to Ala decreases k_{cat} by 25-fold (*43*−*45*). This residue may function as a "lid" to the PLP binding pocket, it may contribute to the electronic properties of PLP, or it may serve as a general acid to provide a proton to the substrate C_α atom after decarboxylation (distance 4 Å, Figure 6). Arg154 interacts with PLP O_3 through a well-ordered water molecule (Figure 6), suggesting that this residue may be important for PLP binding and/or for influencing the tautomeric state of the PLP cofactor.

Correlation of Biochemical Data with the Structure: the Substrate Binding Site. The TbODC structure was solved in a complex with the suicide inhibitor DFMO, which is covalently bound to the enzyme through Cys360. The position and interactions of DFMO likely mimic those of the substrate L-Orn. N_ϵ of DFMO is bound between two acidic residues, Asp361 and Asp332, which are contributed to the active site from opposite subunits. These interactions are likely to be important for substrate discrimination. L-Orn is strongly preferred as a substrate over the longer Lys or shorter α-aminobutyrate (*29*); the k_{cat}/K_m for L-Orn is 100-fold higher than for Lys, and no detectable activity can be measured for α-aminobutyrate. The distance between the Schiff base nitrogen and the Asp361−Asp332 pair may act as a ruler to select for a side chain with length equivalent to the L-Orn. Mutation of Asp361 to Ala increases the K_m for L-Orn by 1000-fold while k_{cat} was essentially unchanged (*40*). The structure suggests that Asp332 is essential for L-Orn binding as well, although no mutant analysis has been performed.

The electron density for DFMO suggests that it is bound in the decarboxylated form, consistent with the reported mechanism of enzyme inactivation (*28*). Thus there is no direct evidence as to the orientation of the carboxylic group for the substrate L-Orn. If we assume that no rotation of the DFMO molecule about the C−N bond occurred after decarboxylation, the prochirality of the DFMO−enzyme complex suggests that the carboxylate would occupy a hydrophobic pocket formed by the side chains of PheB397 and LysA69, behind the PLP molecule (Figure 6). Mutation of Lys69 to Arg decreases the rate of the chemical decarboxylation step by $>10^4$-fold, consistent with a role for this residue in positioning the α-carboxylate for efficient catalysis (*29*). A hydrophobic environment has been demonstrated to enhance both the spontaneous and antibody-catalyzed decarboxylation rates of model molecules (*46*−*48*) and has been proposed to enhance decarboxylation by histidine decarboxylase (*49*). Electrostatic destabilization of the carboxylate group has been proposed to enhance decarboxylation by dialkylglycine decarboxylase (*50*). However, this mechanism is not possible for ODC due to the absence of negatively charged groups in proximity to the DFMO C_α atom.

ODC vs AR: Same Fold, Same Cofactor, Different Reaction Specificity. ODC and AR are homologous PLP-dependent enzymes with different reaction specificity. The PLP system in ODC facilitates decarboxylation, and in AR proton removal/addition occurs at C_α. Comparison of the active sites of ODC and AR might shed some light into how differences in reaction specificity are achieved by the same fold. Several residues in the PLP binding site are invariant in ODC and AR (Figure 1): Lys69/39 forms Schiff base with PLP, His197/166 is positioned in front of the PLP ring, Tyr389/354 and Gly276/221 are involved in phosphate binding, and Cys360/311 is contributed to the active site by the other monomer. However, several striking differences are also found that may contribute to reaction specificity. The N_1 atom of PLP is ligated by Glu274 in ODC, and this interaction is thought to contribute to quinoid stabilization (*40, 51*), required for decarboxylation. In contrast in AR, the N_1 of PLP is ligated by Arg219, possibly disfavoring quinoid formation (*12*). A conserved substitution of two charge pairs between the active sites, Arg154/Lys129 and Lys169/Arg136 (ODC/AR residue), is also found. Arg154 in ODC is involved in a hydrogen-bonding network that includes a well-ordered water molecule and the O_3 of PLP. In the AR structure the distance between the water molecule proximal to O_3 of PLP and Lys129 is 4.7 Å. Arg136 in AR has been proposed to stabilize the substrate carboxylate, as well as interact with the O_3 of PLP (*12, 52, 53*). In ODC the side chain of the corresponding Lys169 is rotated away from the position of the Arg136 side chain in AR, and it forms an interaction with the other monomer (with Asp364), contributing to the dimer interface.

Finally, the amino acid substrate binding sites differ between ODC and AR. In ODC, the L-Orn side chain is stabilized by Asp332 and Asp361. In AR those residues are absent (Figure 1) and a smaller substrate binding pocket is formed in part by Met312 (*52, 53*). In ODC, the corresponding Leu363 is positioned away, making room for the larger L-Orn side chain. Asp361, which binds the N_ϵ of the substrate, is on the loop involved in the hairpin flip (residues 359−364 in ODC and residues 310−313 in AR). In the sequence alignment Cys360/Cys311 is conserved, as are the nearby residues Asp364/Asp313 (ODC/AR). While Cys360/Cys311 are likely to have similar functional roles, Asp364/Asp313 clearly do not. In AR Asp313 is thought to form an ion pair with the Schiff base lysine residue (Lys39) in the course of the reaction (*12, 53*). In ODC Asp364 is in the dimer interface forming an ion pair to the opposite subunit, and the residue(s) that form(s) an ion pair with Lys69 during the reaction has (have) yet to be identified. The buried charge of Asp364 is likely to play a structural role by serving to position the 358−364 hairpin, which includes the active site residues Cys360 and Asp361. The apparent structural role of Asp364 in positioning these active site residues likely explains the severe loss of activity (k_{cat}/K_m is decreased by $>10^5$-fold) observed when this residue is mutated to Ala (*40*).

Dimer Interface. The L-shaped monomers of ODC bury extensive surface area (2775 Å) upon dimer formation. About 17% of residues change their solvation in the dimer versus the monomer. Despite the large buried surface area at the dimer interface, it has been demonstrated that TbODC and mouse monomers are in rapid equilibrium (*14, 45*). While

only 73% of residues in dimer contacts are invariant between mouse and *T. brucei* ODC, cross-species heterodimers between these proteins form readily upon mixing (*14*). These results suggest that determinants of dimerization are invariant and that not all of the side chains in contact between the subunits contribute to the energetics of dimerization equally. In support, the interaction between growth hormone and its receptor is driven by only a few key interactions (*54*). Analysis of buried area per residue demonstrates that Tyr331, Lys169, and Gln166 bury the greatest surface area, more than 100 Å each. A rather interesting feature of a dimer interface is the aromatic zipper, formed by the C-terminal β-barrel domains (Figure 5a). In this structure six aromatic rings are partially stacked together. The structure extends to the active sites where the PLP rings participate in interactions with the end residues in the zipper. The structure suggests that these residues will play a key role in the energetics of dimerization and that they may also help to position PLP for productive catalysis.

There are no salt bridges in the hydrophobic core of the TbODC monomer. However, two buried salt bridges form upon dimerization. These include AspA134/LysB294 and AspB364/LysA169 pairs. The D134A mutant of ODC cannot be expressed in a soluble form (*40*); a decreased ability to dimerize might explain this result. The intersubunit salt bridges are formed on the contact surface between N-terminal and C-terminal domains, near the active site region. Mainly hydrophobic interactions are involved in the contacts of the C-terminal domains with each other. Orienting salt bridges, in combination to less specific hydrophobic interactions, may help in proper positioning of the active site residues at the dimer interface.

In summary, the structure of DFMO bound to the K69A mutant of TbODC has revealed several interesting aspects of the architecture and activity of this PLP-dependent decarboxylase. *T. brucei* ODC is a chemotherapeutic target for the treatment of African sleeping sickness, and this structure will provide the basis for the design of novel inhibitors of the parasite enzyme. This is the first structure of a eukaryotic ODC bound to an inhibitor, and it provides insight into the structural basis for L-Orn specificity and reactivity. DFMO is bound in the subunit interface. The N_ϵ group is bound between two aspartic acid residues (AspA332 and AspB361), and the aliphatic portion rests between AspB361 and TyrA389. The structure further suggests the origin of reaction specificity for decarboxylation. Although the carboxylate group is not observed directly, on the basis of the orientation of DFMO in the active site, the carboxylate likely occupies a hydrophobic pocket formed by the aliphatic portion of LysA69 and PheB397. We hypothesize this hydrophobic pocket promotes neutralization and decarboxylation. In the uncomplexed TbODC and mouse ODC structures, the side chain of Cys360 is rotated away from the active site, positioning the sulfhydryl group too far away to participate in the chemistry of the reaction. In the DFMO-bound TbODC structure, Cys360 is rotated into the active site and is in position to play a catalytic role, either as a general acid or to promote decarboxylation. Comparison of the DFMO-bound and unliganded TbODC structures demonstrates that unlike many PLP-dependent enzymes, no domain or subunit rotations are associated with the binding of ligand to ODC.

ACKNOWLEDGMENT

We thank M. Hackert for providing the coordinates of mouse ODC and D. Ringe for providing the alanine racemase coordinates, both prior to publication; S. Sprang, members of the Sprang laboratory, H. Zhang, and B. Canagarajah for helpful discussions and for aiding in synchrotron data collection; Z. Otwinowski for helpful discussions; the MacChess staff for their assistance with data collection at CHESS; and the staff at the X12C line at the Brookhaven Synchrotron source.

REFERENCES

1. Tabor, C. W., and Tabor, H. (1984) *Annu. Rev. Biochem. 53*, 749−790.
2. Pegg, A. E., Shantz, L. M., and Coleman, C. S. (1995) *J. Cell Biol. 22*, 132−138.
3. McCann, P. P., and Pegg, A. E. (1992) *Pharmacol. Ther. 54*, 195−215.
4. Wang, C. C. (1995) *Annu. Rev. Pharmacol. Toxicol. 35*, 93−127.
5. Bacchi, C. J., Nathan, H. C., and Hunter, S. H. (1980) *Science 210*, 332−334.
6. Kuzoe, F. A. S. (1993) *Acta Trop. 54*, 153−162.
7. Li, F., Hua, S. B., Wang, C. C., and Gottesdiener, K. M. (1996) *Mol. Biochem. Parasitol. 78*, 227−236.
8. Kuntz, I. D. (1992) *Science 257*, 1078−1082.
9. Blundell, T. L. (1996) *Nature 384* (Suppl.), 23−26.
10. Hunter, W. N. (1997) *Parasitology 114*, S17−S29.
11. Grishin, N. V., Phillips, M. A., and Goldsmith, E. J. (1995) *Protein Sci. 4*, 1291−1304.
12. Shaw, J. P., Petsko, G. A., and Ringe, D. (1997) *Biochemistry 36*, 1329−1342.
13. Kern, A. D., Oliveira, M. A., Coffino, P., and Hackert, M. (1999) *Structure 7*, 567−581.
14. Osterman, A. L., Grishin, N. V., Kinch, L. N., and Phillips, M. A. (1994) *Biochemistry 33*, 13662−13667.
15. Grishin, N. V., Osterman, A. L., Goldsmith, E. J., and Phillips, M. A. (1996) *Proteins 24*, 272−273.
16. Jancarik, J., and Kim, S. H. (1991) *J. Appl. Crystallogr. 24*, 409−411.
17. Otwinowski, Z. (1993) *Ocillation data reduction program. Data collection and processing* (Sawyer, L., Isaacs, N., and Bailey, S., Eds.) pp 56−62, Science and Engineering Council, U.K.
18. Navaza, J. (1994) *Acta Crystallogr. A50*, 157−163.
19. Collaborative Computing Project, Number 4 (1994) *Acta Crystallogr. D50*, 760−763.
20. Jones, T. A., and Kjeldgaard, M. (1991) *O version 5.4*, Department of Molecular Biology, Uppsala University, Sweden.
21. Murshudov, G. N., Vagin, A. A., and Dodson, E. J. (1997) *Acta Crystallogr. D53*, 240−255.
22. Brunger, A. T. (1992) *X-PLOR (version 3.1), a system for X-ray crystallography and NMR*, Yale University Press, New Haven, CT.
23. Adams, P. D., Pannu, N. S., Read, R. J., and Brunger, A. T. (1997) *Proc. Natl. Acad. Sci. U.S.A. 94*, 5018−5023.
24. Brunger, A. T. (1992) *Nature 355*, 472−474.
25. Pannu, N. S., and Read, R. J. (1996) *Acta Crystallogr. A52*, 659−668.
26. Laskowski, R. A., MacArthur, M. W., Moss, D. S., and Thornton, J. M. (1993) *J. Appl. Crystallogr. 26*, 283−291.
27. Phillips, M. A., Coffino, P., and Wang, C. C. (1988) *J. Biol. Chem. 263*, 17933−17941.
28. Poulin, R., Lu, L., Ackermann, B., Bey, P., and Pegg, A. E. (1992) *J. Biol. Chem. 267*, 150−158.
29. Osterman, A. L., Brooks, H. B., Jackson, L., Abbott, J. J., and Phillips, M. A. (1999) *Biochemistry 38*, 11814−11826.
30. Kirsch, J. F., Eichele, G., Ford, G. C., Vincent, M. G., and Jansonius, J. N. (1984) *J. Mol. Biol. 174*, 497−525.

31. Swanson, T., Brooks, H. B., Osterman, A. L., O'Leary, M., and Phillips, M. A. (1998) *Biochemistry 37*, 14943−14947.
32. Phillips, M. A., Coffino, P., and Wang, C. C. (1987) *J. Biol. Chem. 262*, 8721−8727.
33. Flores, T. P., Orengo, C. A., Moss, D. S., and Thornton, J. M. (1993) *Protein Sci. 2*, 1811−1826.
34. Chotia, C., and Lesk, A. (1986) *EMBO J. 5*, 823−826.
35. Grishin, N. V. (1997) *J. Mol. Evol. 45*, 359−369.
36. Richardson, J. S. (1981) *Adv. Protein Chem. 34*, 167−339.
37. Abrahams, J. P., Leslie, A. G., Lutter, R., and Walker, J. E. (1994) *Nature 370*, 621−625.
38. Fuentes-Prior, P., Noeske-Jungblut, C., Donner, P., Schleuning, W. D., Huber, R., and Bode, W. (1997) *Proc. Natl. Acad. Sci. U.S.A. 94*, 11845−11850.
39. Murzin, A. G. (1998) *Curr. Opin. Struct. Biol. 8*, 380−387.
40. Osterman, A. L., Kinch, L. N., Grishin, N. V., and Phillips, M. A. (1995) *J. Biol. Chem. 270*, 11797−11802.
41. Onuffer, J. J., and Kirsch, J. F. (1994) *Protein Eng. 7*, 413−424.
42. Osterman, A. L., Brooks, H. B., Rizo, J., and Phillips, M. A. (1997) *Biochemistry 36*, 4558−4567.
43. Tsirka, S., and Coffino, P. (1992) *J. Biol. Chem. 267*, 23057−23062.
44. Tsirka, S. E., Turck, C. W., and Coffino, P. (1993) *Biochem. J. 293*, 289−295.
45. Coleman, C. S., Stanley, B. A., Viswanath, R., and Pegg, A. E. (1994) *J. Biol. Chem. 269*, 3155−3158.
46. Marlier, J. F., and O'Leary, M. H. (1986) *J. Am. Chem. Soc. 108*, 4896−4899.
47. Lewis, C., Paneth, P., O'Leary, M. H., and Hilvert, D. (1993) *J. Am. Chem. Soc. 115*, 1410−1413.
48. Ashley, J. A., Lo, C.-H. L., McElhaney, G. P., Wirsching, P., and Janda, K. D. (1993) *J. Am. Chem. Soc. 115*, 2515−2516.
49. Gallagher, T., Snell, E. E., and Hackert, M. L. (1989) *J. Biol. Chem. 264*, 12737−12743.
50. Toney, M. D., Hohenester, E., Cowan, S. W., and Jansonius, J. N. (1993) *Science 261*, 756−759.
51. Brooks, H. B., and Phillips, M. A. (1997) *Biochemistry 36*, 15147−15155.
52. Stamper, C. G. F., Morollo, A. A., and Ringe, D. (1998) *Biochemistry 37*, 10438−10445.
53. Morollo, A. A., Petsko, G. A., and Ringe, D. (1999) *Biochemistry 38*, 3293−3301.
54. Clackson, T., and Wells, J. A. (1995) *Science 267*, 383−386.
55. Esnousf, B. M. (1997) *J. Mol. Graphics 15*, 133−138.
56. Kraulis, P. J. (1991) *J. Appl. Crystallogr. 24*, 946−950.
57. Nicholls, A., Bharadwaj, R., and Honig, B. (1993) *Biophys. J. 64*, A166−A166.

BI9915115